Oriented Aggregation and Novel Phase Transformation of Vaterite Controlled by the Synergistic Effect of Calcium Dodecyl Sulfate and *n*-Pentanol

Qiang Shen,*,† Liancheng Wang,† Yaping Huang,‡ Jinglun Sun,† Haihua Wang,† Yong Zhou,‡ and Dujin Wang‡

Key Laboratory for Colloid and Interface Chemistry of Education Ministry, School of Chemistry & Chemical Engineering, Shandong University, Ji'nan 250100, China, and State Key Laboratory of Polymer Physics & Chemistry, Institute of Chemistry, Chinese Academy of Sciences, Beijing 100080, China

Received: June 28, 2006; In Final Form: August 18, 2006

Calcium dodecyl sulfate (CDS) was used for the first time both as an anionic surfactant and as the source of mineral ions in the precipitation process of calcium carbonate ($CaCO_3$). The simple reaction of the enriched Ca^{2+} ions at the so-called organic−inorganic interfaces with the slowly bubbled CO_2 gas resulted in the metastable vaterite polymorph with various structures. The single-crystalline vaterite of the hexagonal platelets, the lens-shaped structures with hexagonal symmetry, the olive-shaped superstructures and these with a concave at each top of olives, and another metastable polymorph of aragonite were obtained, respectively, depending upon the concentration ratio between CDS and *n*-pentanol. The synergistic effect of CDS and *n*-pentanol is believed to play a crucial role in driving the oriented aggregation of metastable nanoparticles. Simultaneously, the novel phase transformation of vaterite to aragonite was observed, implying the possible formation mechanism of aragonite at room temperature and in the absence of magnesium ions.

1. Introduction

During the controlled crystal morphogenesis in organisms (i.e., the biomineralization), biomaterials with complex structures and properties can be formed in water at ambient temperature.[1−3] Also, various formation mechanisms are speculated, for example the interfacial recognition (or the polymorphic selectivity) and the oriented aggregation of nanoparticles.[4,5] However, organisms should initially enrich and/or extract the elements needed from the local environment. Then, the biomolecules and their self-organized structures can cooperate with the deposited minerals into functionalized structures under strict biological control.[2] One of the most surprising phenomena in biomineralization is the formation and stabilization of single-crystalline minerals with hierarchical structures and in the thermodynamically unstable form.[3] Such self-organized superstructures, if fabricated synthetically, could have numerous important applications.[4] A promising approach is to use organic additives and/or templates to control the nucleation, growth, and alignment of inorganic materials, which have received much attention in recent years.[5]

Calcium carbonate ($CaCO_3$) is one of the most common biological minerals, and it has polymorphs of calcite, aragonite, and to a lesser extent in the amorphous state, vaterite and monohydrate in calcareous structures of organisms.[6] While in the precipitation process of $CaCO_3$, the size, shape, and structure of the products depend on the experimental conditions.[7] Although lots of organic compounds have been used to synthesize $CaCO_3$ crystals and to control their morphologies, polymorphs, and metastable phases,[8] it is also very difficult to make it clear what is the real manipulation process of organics in biomineralization. For example, the headgroups of sodium dodecyl sulfate (SDS) could act as active sites for $CaCO_3$ nucleation, due to their electrostatic interaction with calcium ions.[9,10] Then, the presence of SDS influenced the crystal growth, polymorphic transformation, and particle aggregation of $CaCO_3$, which is mainly due to the SDS molecule adsorption onto $CaCO_3$ surfaces.[9b]

In the rapid mixing of $CaCl_2$ and Na_2CO_3 solutions, the organic precursor of SDS micelles cooperated with the deposited calcite particles to form the core−shell structure.[10a] The phenomenon of molecular recognition or shape control is probably one of the basic principles in biomineralization. Interestingly, in the slow titrating process of $CaCl_2$ into the aqueous SDS micellar solution containing Na_2CO_3, the obtained $CaCO_3$ crystals were a mixture of calcite and aragonite at room temperature and in the absence of magnesium ions.[10b] Similar results often occur in some biomimetic mineralization (or biomineralization), but in the presence of acidic macromolecules (or acidic proteins) and/or magnesium ions.[11] If the sodium ions of SDS molecules were replaced by calcium ions, the resulted double-chain surfactants of CDS could be used both as the organic additives and as the source of calcium ions in the precipitation of $CaCO_3$. The bound calcium ions on the surface of CDS self-assemblies simulate, more or less, the selective enrichment and/or extraction of mineral elements in biomineralization. Then, the slow dissolving of CO_2 gas into the aqueous CDS systems, and the subsequent crystallization and aggregation processes of inorganic minerals, could also, to some extent, account for the formation mechanism of the in vivo functionalized structures.

In this paper, bivalent metal dodecyl sulfate of CDS was synthesized and used in the precipitation process of $CaCO_3$. The synergistic effect of CDS and *n*-pentanol on the crystallization habit of $CaCO_3$ and the oriented aggregation of vaterite was investigated. Aside from these, another interesting phenomenon for the phase transformation of vaterite to aragonite was found, which was seldom observed in the synthetic processes of $CaCO_3$ materials. Perhaps this implies the formation mechanism of the brickwall-typed nacreous layer, composed of aragonite tablets, which occurred at room temperature and in the absence of magnesium ions.

* Corresponding author. Phone.: +86-531-88361387. Fax: +86-531-88564750. E-mail: qshen@sdu.edu.cn.

† Key Laboratory for Colloid and Interface Chemistry of Education Ministry.

‡ State Key Laboratory of Polymer Physics & Chemistry.

10.1021/jp064039n CCC: $33.50
Published on Web 10/21/2006

2. Experimental Section

2.1. Materials. All chemicals, sodium dodecyl sulfate (SDS), calcium chloride, *n*-pentanol, and ammonia ($NH_3 \cdot H_2O$), are of A. R. grade and were used without further purification. Carbon dioxide (CO_2, 99.99%) was purchased from Jinan Deyang Special Gas Co. Ltd. (Jinan, China). Deionized water was used throughout the sample preparations. Calcium dodecyl sulfate (CDS) was synthesized by reacting 100 g of SDS with 34 g of $CaCl_2$ in 1 L of deionized water.[12,13] The CDS precipitate that formed was filtered through cellulose nitrated/acetate membrane (0.22 μm) and fully rinsed with deionized water. After recrystallization from water three times, the obtained CDS was dried in a vacuous desiccator at room temperature. The purity of the CDS sample was ascertained by the absence of the minimum in the surface tension curve measured at 55 °C.

2.2. $CaCO_3$ Precipitation Experiments. The surfactant, CDS, was used as the source of calcium ions, and the CO_2-diffusion precipitation method was used to prepare calcium carbonate ($CaCO_3$). First, a 50 g solution containing CDS (1.9 $\sim$ 3.5 wt %), *n*-pentanol (1.5 $\sim$ 3.0 wt %), and a definite concentration of ammonia was prepared and homogenized in a 50-mL beaker. The amount of ammonia was chosen at a fixed molar ratio of CDS to $NH_3 \cdot H_2O$ (1: 4). Then, the freshly prepared solution reacted with CO_2 gas that was introduced to the sublayer of the air/solution interface through a glass capillary.

The flow rate of CO_2 gas was fixed at ca. 2.5 mL/min, and the inpouring time was 1 h unless it was otherwise described in the text. The pH value of the reactive solution was measured by a combination electrodes Mettler Toledo HA405-K2/120 $\pm$ 0.01 pH) which was calibrated before each experiment by the two standard buffer solutions of tartrate (25 °C, pH = 3.56) and borate (25 °C, pH = 9.18). Before and/or after CO_2-inpouring, the pH of the reactive systems did not change with time, depending upon the amount of the added ammonia. Nevertheless, during the CO_2-inpouring period the pH value decreased from 11.3 ± 0.3 ($t = 0$ min) to 9.3 ± 1.2 ($t = 60$ min).

During the CO_2-inpouring period, the precipitation systems were stirred at a constant rate of 200 rpm by the Teflon-coated magnetic stir bar, keeping the homogeneity of ion intensity and of pH value. Then, the resulting $CaCO_3$ particles were kept still in the incubation systems for 24 h to allow further crystal growth by Ostwald ripening, unless it was otherwise described in the text. After being filtered through cellulose nitrated/acetate membrane filters (0.22 μm) and rinsed three times with the mixture of ethanol and water (50 : 50, v/v), the $CaCO_3$ crystals were dried in a vacuous desiccator cabinet at room temperature for 24 h and used for measurements.

2.3. Crystal Caracterization. All samples were Au-coated prior to examination by a Hitachi S-4300 scanning electron microscope (SEM), fitted with a field emission source and operated at an accelerating voltage of 15 kV.

Transmission electron microscopy (TEM) images were recorded by a Hitachi H-800 transmission electron microscope operating at 200 kV. The samples dispersed in ethanol were directly deposited on a carbon film supported by a copper grid.

The X-ray diffraction (XRD) patterns were collected on a Rigaku D/max-2400 powder X-ray diffractometer with Cu Kα radiation (40 kV, 120mA). The 0.02° steps/(25 s) and the 2θ range from 20° to 60° were selected to analyze the crystal structure and orientation.

The Fourier transform infrared (FT IR) spectrum measurements were performed on a Bruker IFS 100 FT-Raman spectrometer with the resolution of 4 cm^{-1}.

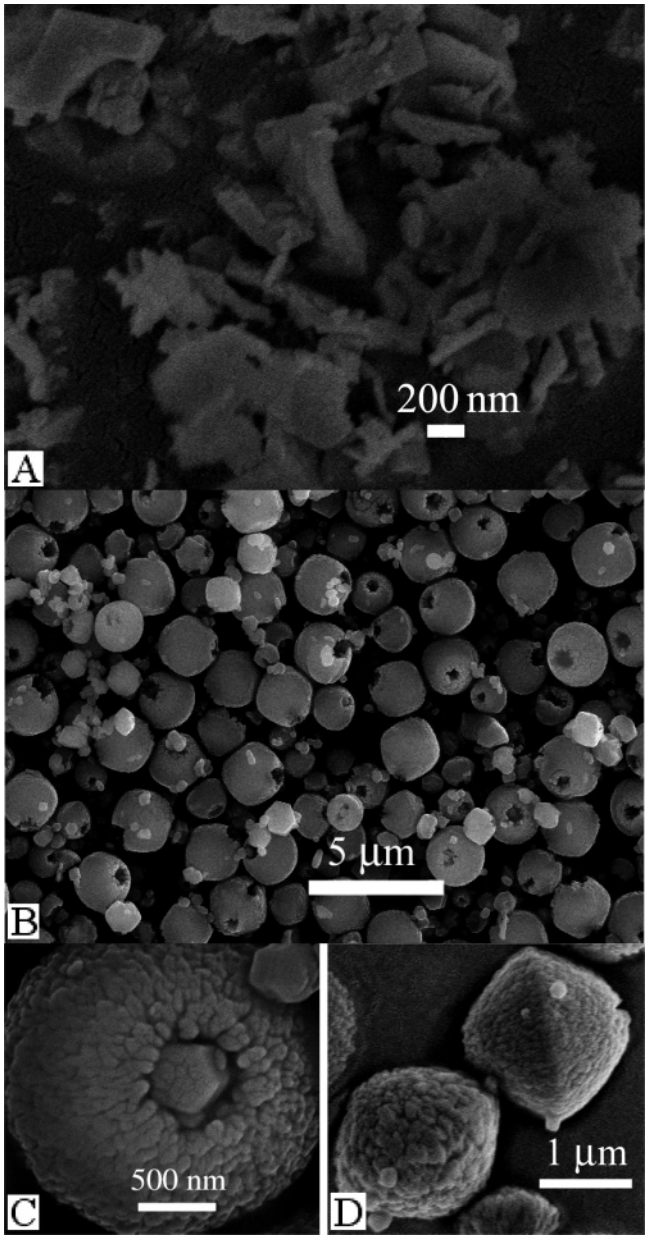

Figure 1. SEM images of the $CaCO_3$ crystals precipitated from the CDS (2.0 wt %) micellar solutions in the absence (A) and presence (B, C, and D) of *n*-pentanol (2.5 wt %) at the aging time of 24 h.

3. Results and Discussion

3.1. Morphological Effect of the Concentration Ratio of CDS to *n*-Pentanol. CDS is insoluble both in water and in *n*-pentanol at room temperature. However, it can be dissolved in the mixture of water and *n*-pentanol, forming an isotropic micellar phase.[14] Because CDS behaves like a two-chain nonionic surfactant,[14] the addition of ammonium has nearly no influence on the phase behavior of the aqueous systems containing the mixed micelles of CDS and *n*-pentanol. The Krafft point of CDS is 50 °C,[13a] and the critical micellization concentration (CMC) of the synthesized CDS was $\sim 1.0 \times 10^{-3}$ M, coinciding with the value described in ref 13b. In the precipitation of $CaCO_3$, CO_2 gas was bubbled, for 1 h, into the CDS micellar system in the absence of *n*-pentanol at 55 °C. Then, the reactive solution was allowed to stand still at room temperature for 24 h. The resulting particles were characterized by SEM and FT IR methods, which were shown in Figures 1A and 2A.

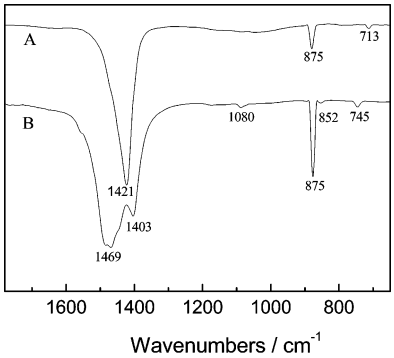

Figure 2. FT IR spectra of the $CaCO_3$ crystals precipitated from the CDS (2.0 wt %) micellar solutions in the absence (A) and presence (B) of *n*-pentanol (2.5 wt %) at the aging time of 24 h.

Figure 1A shows the lengthened or fractional particles of rhombohedrons. Also, the corresponding FT IR spectrum (Figure 2A) presents the calcite characteristic adsorption peaks at 1421 (ν_3), 875 (ν_2), and 713 (ν_4) cm^{-1}, respectively.[15] It has been proven in the literature[9b,16] that a surfactant presented in the systems can influence the nucleation, crystal growth, and aggregation of the particles. Herein, the presence of CDS micelles only resulted in calcite, which could be used as a control for the mixed micelles of CDS and *n*-pentanol. However, the precipitation of $CaCO_3$ in the presence of CDS micelles was conducted at 55 °C, while that in the presence of the mixed micelles was performed at room temperature. This was due to the smaller solubility product of CDS than those of various $CaCO_3$ solids at ambient temperatures.[17]

At room temperature, the olive-shaped superstructures of $CaCO_3$ crystals (Figure 1B) were obtained by introducing CO_2-gas into the aqueous solutions containing the mixed micelles of CDS and *n*-pentanol. The top view (Figure 1C) and side view (Figure 1D) of these aggregates at high resolution also suggest the oriented attachment of nanoparticles. Interestingly, these superstructures (Figure 1B−D) have a concave feature, not the hole detected by TEM method, on each top of the olive-shaped structures.

The FT IR spectrum of these $CaCO_3$ superstructures (Figure 2B) exhibits a split adsorption peak at 1469 and 1403 cm^{-1}, and the characteristic adsorption peaks of vaterite at 1080 (ν_1), 875 (ν_2), and 745 (ν_4) cm^{-1}, respectively.[15] Although no aragonite crystals were observed in Figure 1B, the adsorption peak at 852 cm^{-1} can be assigned to ν_2 of aragonite.[10b] However, the preferential nucleation of vaterite in the presence of CDS and *n*-pentanol, as well as the pure calcite product in the absence of *n*-pentanol, suggests that there is a synergistic effect of CDS and *n*-pentanol on the kinetic promotion of the metastable polymorph. It should be emphasized that the split peak in Figure 2B can be assigned to the ν_3 characteristics of amorphous calcium carbonate,[7b] indicating the partly amorphous nature of these vaterite aggregates. And, this indicates that the formation of the concaves was probably due to the dissolution of the amorphous phase or vaterite, or both.

Generally, increased incorporation of medium-chain alcohol molecules could reduce the packing parameter of surfactants continuously.[14] Herein, the change of the concentration ratio of CDS to *n*-pentanol should change the distance among CDS headgroups at the so-called organic/inorganic interface. Consequently, it can modify to some extent their synergistic effectiveness on $CaCO_3$ particle morphology. Figure 3A−C shows the morphological evolvement of the $CaCO_3$ crystals precipitated from 2.0 wt % CDS solutions containing different *n*-pentanol concentration of 1.5 (A), 1.75 (B), and 2.0 (C),

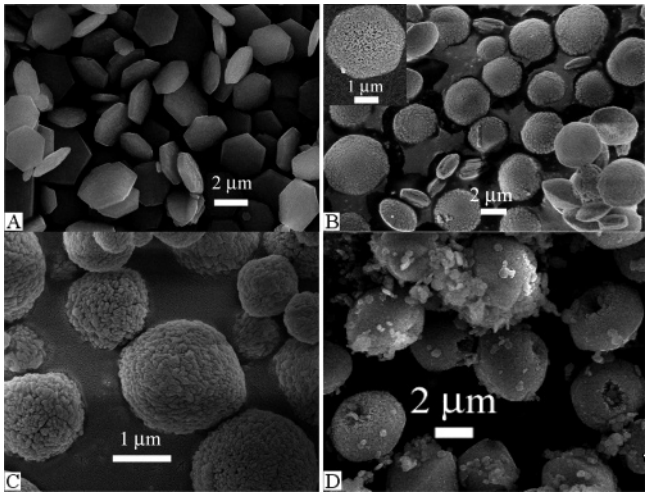

Figure 3. SEM images of the $CaCO_3$ crystals precipitated from 2.0 wt % CDS solutions in the presence of 1.5 (A), 1.75 (B), and 2.0 (C) wt % *n*-pentanol, respectively, at the aging time of 24 h. The inset is the magnified SEM picture of a lens-shaped vaterite. Panel D presents the SEM image for the $CaCO_3$ crystals precipitated from the aqueous solutions of 1.9 wt % CDS + 1.9 wt % *n*-pentanol at the same incubation time.

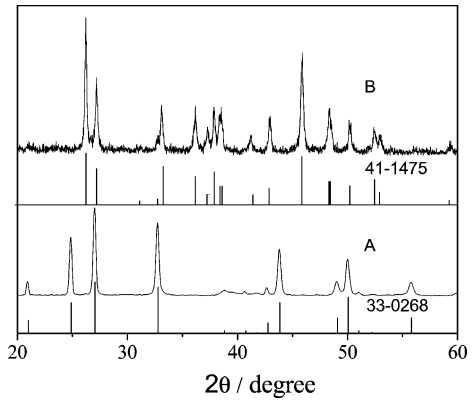

Figure 4. XRD spectra for the $CaCO_3$ particles sampled from the aqueous solutions of 2.0 wt % CDS + 2.5 wt % *n*-pentanol at the different intervals of 24 h (A) and 48 h (B), respectively. The nether lines correspond to the standard position and the relative intensities for the randomly oriented crystals of vaterite (JCPDS 33-0268) and aragonite (JCPDS 41-1475), respectively.

respectively. Figure 3D is the SEM picture of the $CaCO_3$ crystals sampled from the aqueous system of 1.9 wt % CDS + 1.9 wt % *n*-pentanol. These collected crystals, shown in Figures 1B and 3, exhibit the same XRD characteristics as those shown in Figure 4A. The nether lines below Figure 4A belong to the standard position and the relative intensities of the randomly oriented vaterite (JCPDS 33-0268).[18] It should be emphasized that (1) it is almost impossible to detect the amorphous $CaCO_3$ by the XRD instrument;[7b] and (2) there is the possibility that the content of one crystalline form was too small to be detected. So, the coincidence of the XRD spectrum (Figure 4A) with its nether line only indicates predominantly the crystalline nature of vaterite.

In the presence of *n*-pentanol (1.5 wt %), the distance among CDS headgroups might favor the nucleation of the (001) plane of vaterite crystals, modifying the growth stage and creating sharp edges and the hexagonal platelets (Figure 3A). Although similar results have been observed by using surfactants,[10b, 15b] a stearate Langmuir monolayer,[19a] polymers,[19b] or NH_3,[20] it is also very difficult to explain why only the hexagonal platelets were obtained under this condition. The increase of *n*-pentanol

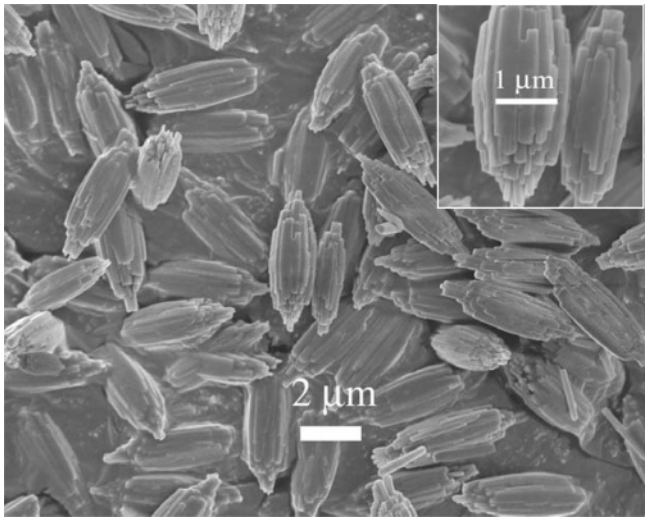

Figure 5. SEM image of the $CaCO_3$ particles precipitated from the aqueous solutions of 2.0 wt % CDS + 2.5 wt % *n*-pentanol at the aging time of 48 h. The inset is the magnified picture of the $CaCO_3$ bundles.

concentration (1.75 wt %) changed the morphology of vaterite crystals, showing the lens-shaped structures with hexagonal symmetry (Figure 3B). The inset in Figure 3B shows the rough or the porous nature for the lens surface. Then, with the continuous addition of *n*-pentanol up to the concentration ratio of 1:1 (CDS/*n*-pentanol, wt/wt), the olive-shaped superstructures without concaves were obtained (Figure 3C).

It should be pointed out that when the *n*-pentanol concentration was fixed at 2.5 wt %, the change in the CDS concentration (∼1.9−3.5 wt %) only resulted in the olive-shaped superstructures with a concave at each top (data omitted). Herein, another complex superstructure of vaterite aggregates (Figure 3D) should also be specified. This superstructure seems to be the intermediate between the olives shown in Figure 1B and the lens shown in Figure 3B, implying the oriented aggregation of vaterite nanoparticles.

3.2. Phase Transformation of Vaterite to Aragonite. The initially formed $CaCO_3$ solids belong to the amorphous phase, which is transformed within a few minutes to a crystalline mixture of vaterite and calcite, at a low-temperature period ranging from 14 to 30 °C. Then, the formed vaterite will be transformed into calcite by a solution-mediated process.[7a] The comparison of the vaterite superstructures shown in Figure 3C with these shown in Figure 1B seems to suggest that concaves were formed due to the dissolution of vaterite.

Figure 5 is the SEM picture of the $CaCO_3$ crystals obtained from the reaction system of 2.0 wt % CDS + 2.5 wt % *n*-pentanol at the aging time of 48 h, showing the olive-shaped superstructures with a large aspect ratio. The inset in Figure 5 clearly shows that these superstructures are composed of $CaCO_3$ needles. The corresponding XRD was shown in Figure 4B, exhibiting only the typical reflection peaks of aragonite and coinciding well with the standard position and the relative intensities of the randomly oriented aragonite (JCPDS 41-1475).[18] Here, we would like to cite Bujan's results:[21] at a concentration above the CMC, the electrostatic adsorption of dodecyl sulfate anions (DS^-) on the crystal faces could induce the phase change of calcium hydrogen phosphate dihydrate. In Bujan's opinion, the appearance of the 852 cm^{-1} adsorption peak in Figure 2B further validated that the novel phase transformation of vaterite to aragonite existed in these systems.

To certify the phase transformation process, the time-course

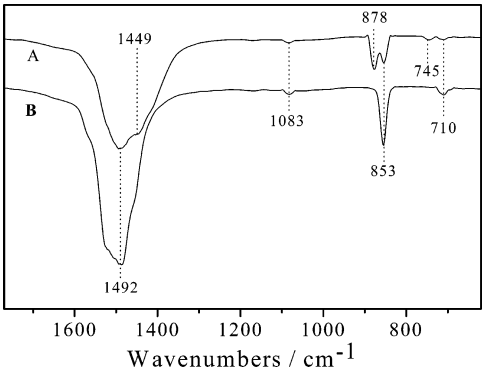

Figure 6. FT IR spectra for the $CaCO_3$ particles precipitated from the aqueous solution of 2.0 wt % CDS + 3.0 wt % *n*-pentanol at the aging times of 24 (A) and 48 h (B), respectively.

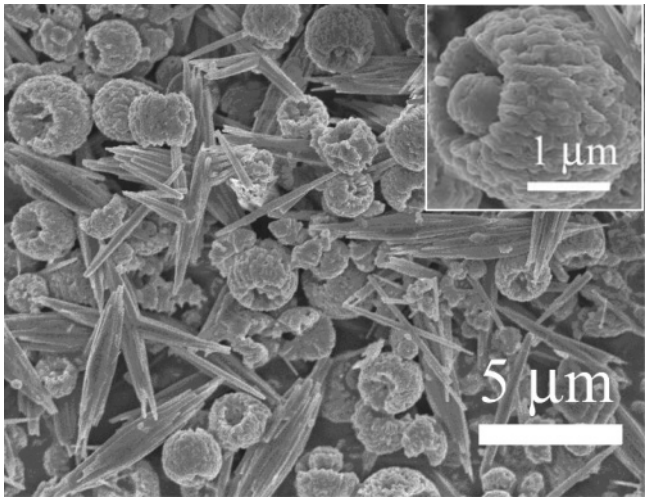

Figure 7. SEM image of the $CaCO_3$ crystals precipitated from the aqueous solution of 2.0 wt % CDS + 3.0 wt % *n*-pentanol at the aging time of 24 h.

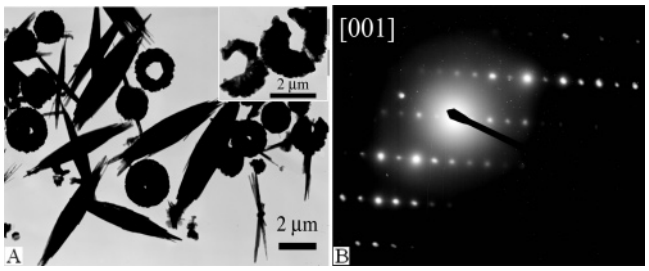

Figure 8. TEM images (A) of the $CaCO_3$ crystals precipitated from the aqueous solution of 2.0 wt % CDS + 3.0 wt % *n*-pentanol at the aging time of 24 h. The inset is the TEM picture for the dissolving vaterite particles. Panel B shows the corresponding electron diffractions selected on the tip areas of aragonite.

experiments for the reaction systems of 2.0 wt % CDS + 3.0 wt % *n*-pentanol were conducted, which are shown in Figures 6−8. Figure 6 shows the FT IR results for the $CaCO_3$ sampled at different intervals, exhibiting the characteristic adsorption peaks of aragonite at 710, 853, and 1083 cm^{-1} (Figure 6A,B), respectively.[10b,22] When the $CaCO_3$ had been incubated for 48 h, its FT IR spectrum shows a vibrational band at 1492 cm^{-1} (Figure 6B), which should be assigned to the asymmetric C−O stretch absorption for aragonite.[22] While for the $CaCO_3$ particles sampled at the aging time of 24 h, the corresponding FT IR spectrum (Figure 6A) also present the characteristic peaks of vaterite at 745 and 878 cm^{-1}. The adsorption band at 1449 cm^{-1} could be referred as the shoulder of 1492 cm^{-1} peak (Figure

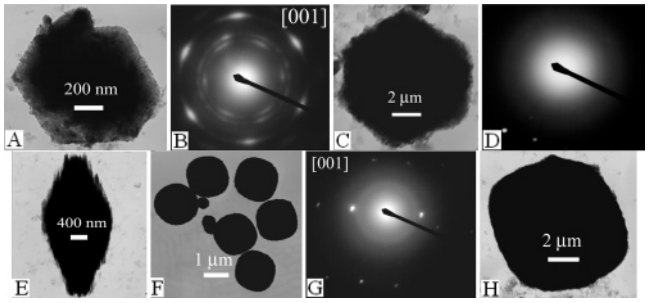

Figure 9. TEM results of the $CaCO_3$ crystals precipitated from the aqueous solution of 2.0 wt % CDS + 2.5 wt % *n*-pentanol. The isolated $CaCO_3$ particles shown in the panels of A, C, E, and F were obtained immediately after various CO_2-inpouring times of 30 (A), 40 (C), 50 (E), and 60 min (F), respectively. Panels B, D, and G represent the corresponding SAED patterns for samples A, C, and E, respectively. Panel H shows the TEM image of the typical $CaCO_3$ particle obtained at the aging time of 24 h.

6A), which resembles the uncertain ν_3 absorption peak of the amorphous $CaCO_3$.[10b] The disappearance of vaterite at the incubation time of 48 h confirms that the metastable aragonite particles resulted from the dissolution of vaterite.

At the aging time of 24 h, the anamorphic particles of vaterite superstructures and spindle-shaped aggregates of aragonite coexisted in the system (Figure 7). The inset in Figure 7 shows that the surfaces of vaterite particles are rougher than these shown in Figure 1B−D, indicating the dissolution of vaterite. Fortunately, the big holes and/or concaves of vaterite particles were detected by TEM observations (Figure 8A, and its inset). The SAED patterns focused on the building blocks of aragonite aggregates (Figure 8B) clearly indicate that the long axis of the crystal is the single-crystalline face of [001]. So, it was the phase transformation of vaterite to aragonite that caused the formation of defects for the olive-shaped vaterite superstructures.

By the results listed above, the synergistic effect of CDS and *n*-pentanol can change the normal phase transformation from vaterite to calcite to the novel one from vaterite to aragonite, especially in the presence of high *n*-pentanol concentration (3.0 wt %). This also implies, to some extent, the in vivo formation mechanism of metastable aragonites at room temperature and in the absence of magnesium ions.

3.3. Formation Mechanism of the Olive-Shaped Vaterite Superstructures. There are two formation mechanisms for the crystal growth in solution systems: the basic one is the well-known Ostwald ripening, and another is the oriented aggregation (or the oriented attachment).[23] Normally, the oriented aggregation of nanoparticles into ordered structures is mainly directed by a special binding interaction of the bridging ligands capped on the surface of nanoparticles. However, recent studies revealed that the self-aggregation of the unstabilized nanoparticles can be controlled, modifying the crystallization process and/or the phase transformation of the amorphous phase.[24] To unravel the formation mechanism of the olive-shaped vaterite superstructures, the precipitates sampled at various intervals were investigated by a TEM method (shown in Figure 9).

During the CO_2-inpouring period, the dissolved CO_2 (or the resulting CO_3^{2-} ions) reacted with the Ca^{2+} ions bound to the surface of "the mixed monolayers of CDS and *n*-pentanol", resulting in the initially formed $CaCO_3$ particles capped by organic molecules.[7,14] Then, the synergistic effect of surfactant and cosurfactant promoted the formation of the hexagonal platelets of vaterite (Figure 9A), confirmed by the selected area electron diffraction (SAED) pattern (Figure 9B).[10b] If the continuously formed amorphous $CaCO_3$ were deposited onto

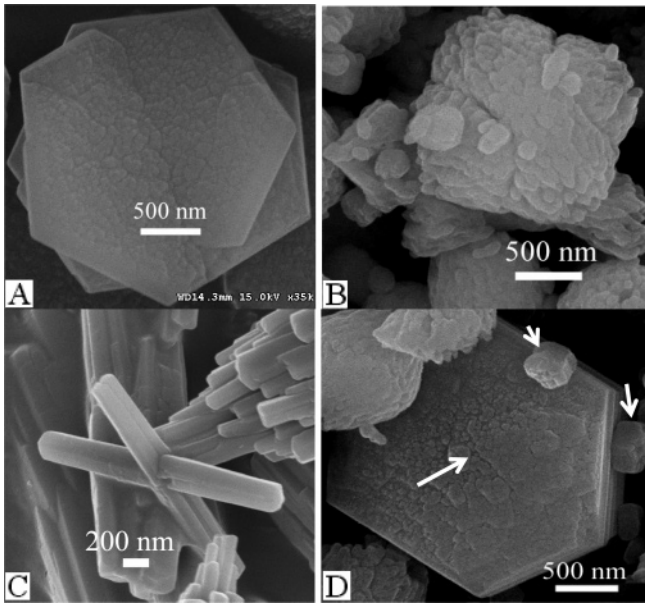

Figure 10. SEM images of the unusual $CaCO_3$ crystals obtained at different CDS (wt %)/*n*-pentanol (wt %) concentration ratios of 2.0/1.5 (A), and 2.0/2.5 (B−D), respectively. Panels A, B, and D show the symbiotic particles sampled at the aging time of 24 h, while panel C shows the intergrowth of aragonite obtained at the aging time of 48 h. Arrows indicate the hexagonal prism of vaterite.

the surface of the vaterite hexagons, driven by the minimizing surface energy,[25] then consequently, the resulting hexagonal platelets became bigger in size and acquired rough surfaces (Figure 9C). When the TEM electron beam was focused on the edge of the hexagonal platelet (Figure 9C), the corresponding SAED pattern (Figure 9D) indicates the partly amorphous nature of the vaterite particle.

It can also be imaged that, if the continuously transformed nanoparticles of vaterite were gradually attached onto the [001] face of the single-crystalline vaterite in perpendicular direction, the olive-shaped superstructures (Figure 9E and 9F) could be obtained at the longer CO_2-inpouring time. It was occasionally observed that the superstructure with the large aspect ratio generated tips on each top (Figure 9E). Interestingly, the corresponding SAED pattern focused on the tips showed the [001] face of the aragonite crystal (Figure 9G), indicating the beginning for the vaterite−aragonite transformation at an early stage. After 1 h of CO_2-inpouring, the obtained $CaCO_3$ particles were incubated in the bulk phase to examine the formation process of concaves mentioned above. Figure 9F shows that no concaves exist for the olive-shaped superstructures sampled at the aging time of 0 h, consistent with that described in Figure 3C. Then, defects appeared on each of the tops of vaterite superstructures (Figure 9H), indicating that concaves resulted from the dissolution of vaterite.

According to Penn's opinion, oriented attachment is a special case of aggregation that provides an important route by which nanocrystals grow, and unique, often symmetry-defying, crystal morphology are produced.[23a] Despite the specific self-assembly of primary nanocrystals, single-crystalline particles, twins, and/or intergrowths can possibly be formed.[23a] Fortunately, the unusual $CaCO_3$ crystals produced from the above reactive systems were directly captured under SEM observation, which was shown in Figure 10.

Figure 10A presents one intergrowth of hexagonal platelets occasionally obtained from the precipitation system containing 2.0 wt % CDS and 1.5 wt % *n*-pentanol. If the primary vaterite nanoparticles were gradually attached onto the [001] faces of

the vaterite intergrowth (shown in Figure 10A) in the perpendicular direction, and then, another intergrowth of the olive-shaped superstructures resulted by means of the oriented aggregation mechanism (Figure 10B). If the symbiotic phenomenon occurred during the formation process of aragonite, the intergrowth of needle-shaped crystals could also be observed (Figure 10C). It should be mentioned that, during the formation process of the olive-shaped vaterite superstructures, hexagonal prisms of $CaCO_3$ crystals were obtained (Figure 10D). From the above discussion, it was concluded that the oriented aggregation mechanism accounted for the formation of the olive-shaped superstructures.

4. Conclusions

The functionalized surfactant of CDS was prepared and used for the first time in the precipitation of $CaCO_3$. The bound counterions to the mixed monolayer of surfactant and cosurfactant partly simulate the element uptake of calcium from the environment in biomineralization. Then, the slow CO_2-inpouring was conducted to synthesize the vaterite crystals with complex structures. The oriented aggregation process accounts for the formation mechanism of the olive-shaped vaterite superstructures. The synergistic effect of CDS and *n*-pentanol was believed to play an important role in the polymorphic selectivity of the metastable vaterite and, furthermore, in the novel phase transformation of vaterite to aragonite at room temperature and in the absence of magnesium ions. These results might not only shed light on the in vivo mineralization, but might also provide an important approach to the fabrication of the special materials with improved performances.

Acknowledgment. The financial support from the Natural Science Found of Shandong Province (Y2004B05), the Excellent Young Scientist Awarding Fund of Shandong Province (02BS115), and the National Natural Science Foundation of China (20471064) are gratefully acknowledged.

References and Notes

(1) (a) Currey, J. D. *J. Zool. London* **1976**, *180*, 445−453. (b) Currey, J. D. *Proc. R. Soc. London, Ser. B* **1977**, *196*, 443−463. (c) Currey, J. D. *J. Zool. London* **1979**, *188*, 301−308. (d) Currey, J. D. *The Mechanical Properties of Biological Materials*; Vincent, J. F. V., Currey, J. D., Ed.; Cambridge University Press: Cambridge, U. K.. 1980; pp 75−97.

(2) Mann, S. *Biomineralization-Principles and Concepts in Bioinorganic Materials Chemistry*; Compton, R. G., Davies, S. G., Evans, J., Ed.; Oxford University Press: Oxford, 2001; pp 1−5.

(3) (a) Addadi, L.; Aizenberg, J.; Benash, E.; Weiner, S. In *Crystal Engineering*—From Molecules and Crystals to Materials; Braga, D., Grepioni, F., Orpen, A. G., Ed.; Kluwer Academic Publishers: Dordrecht, The Netherlands, 1999; pp 1−22. (b) Aizenberg, J.; Lambert, G.; Weiner, S.; Addadi, L. *J. Am. Chem. Soc.* **2002**, *124*, 32−39.

(4) (a) Cölfen, H.; Mann, S. *Angew. Chem., Int. Ed.* **2003**, *42*, 2350−2365. (b) Yu, J. G.; Yu, J. C.; Zhang, L. Z.; Wang, X. C.; Wu, L. *Chem. Commun.* **2004**, 2414−2416.

(5) (a) Cölfen, H.; Antonietti, M. *Angew. Chem., Int. Ed.* **2005**, *44*, 2−17. (b) Zhan, J. H.; Lin, H. P.; Mou, C. Y. *Adv. Mater.* **2003**, *15*, 621−623. (C) Aizenberg, J.; Black, A. J.; Whitesides, G. M. *J. Am. Chem. Soc.* **1999**, *121*, 4500−4509.

(6) Watabe, N. In *Progress in Crystal Growth Characterization*; Pamplin, B. R., Ed.; Pergamon Press: New York, 1981; Vol. 4, pp 99−147.

(7) (a) Wei, H.; Shen, Q.; Zhao, Y.; Wang, D.-J.; Xu, D.-F. *J. Cryst. Growth* **2003**, *250*, 516−524. (b) Shen, Q.; Wei, H.; Zhou, Y.; Huang, Y. P.; Yang, H. R.; Wang, D. J.; Xu, D. F. *J. Phys. Chem. B* **2006**, *110*, 2994−3000.

(8) (a) Donners, J. J. J. M.; Nolte, R. J. M.; Sommerdijk, N. A. J. M. *J. Am. Chem. Soc.* **2002**, *124*, 9700−9701. (b) Ajikumar, P. K.; Wong, L. G.; Subramanyam, G.; Lakshminarayanan, R.; Valiyaveettil, S. *Cryst. Growth Des.* **2005**, *5*, 1129−1139.

(9) (a) Leontidis, E.; Kyprianidou-Leodidou, T.; Caseri, W.; Robyr, P.; Krumeich, F.; Kyriacou, K. C. *J. Phys. Chem. B* **2001**, *105*, 4133−4144. (b) Chibowski, E.; Szczes, A.; Holysz, L. *Langmuir* **2005**, *21*, 8114−8122.

(10) (a) Shen, Q.; Wei, H.; Wang, L.; Zhou, Y.; Zhao, Y.; Zhang, Z.; Wang, D.; Xu, G.; Xu, D. *J. Phys. Chem. B* **2005**, *109*, 18342−18347. (b) Wei, H.; Shen, Q.; Zhao, Y.; Wang, D. J.; Xu, D. F. *J. Cryst. Growth* **2004**, *260*, 545−550.

(11) (a) Hosoda, N.; Sugawara, A.; Kato, T. *Macromolecules* **2003**, *36*, 6449−6452. (b) Küther, J.; Seshadri, R.; Knoll, W.; Tremel, W. *J. Mater. Chem.* **1998**, *8*, 641−650.

(12) (a) Zapf, A.; Hammel, R.; Platz, G. *Colloids Surf., A* **2001**, *183−185*, 213−225. (b) Moroi, Y.; Motomura, K.; Matuura, R. *J. Colloid Interface Sci.* **1974**, *46*, 111−117.

(13) Miyamoto, S. *Bull. Chem. Soc. Jpn.* **1960**, *33*, 372−375. (b) Miyamoto, S. *Bull. Chem. Soc. Jpn.* **1960**, *33*, 375−378.

(14) (a) Hornfeck, U.; Gradzielski, M.; Mortensen, K.; Thunig, C.; Platz, G. *Langmuir* **1998**, *14*, 2958−2964. (b) Zapf, A.; Hornfeck, U.; Platz, G.; Hoffmann, H. *Langmuir* **2001**, *17*, 6113−6118.

(15) (a) Xu, X.; Han, J. T.; Cho, K. *Chem. Mater.* **2004**, *16*, 1740−1746. (b) Dupont, L.; Portemer, F.; Figlarz, M. *J. Mater. Chem.* **1997**, *7*, 797−800.

(16) (a) Heywood, B. R.; Mann, S. *Chem. Mater.* **1994**, *6*, 311−318. (b) Wei, H.; Shen, Q.; Zhao, Y.; Zhou, Y.; Wang, D.; Xu, D. *J. Cryst. Growth* **2004**, *264*, 424−429.

(17) (a) Elfil, H.; Roques, H. *Desalination* **2001**, *137*, 177−186. (b) Zapf, A.; Beck, R.; Hoffmann, H. *Adv. Colloids Interface Sci.* **2003**, *100−102*, 349−380.

(18) The standard XRD spectra for randomly oriented crystals of vaterite (JCPDS 33-0268) and aragonite (JCPDS 41-1475) in the manipulation software of the Rigaku D/max-2400 powder X-ray diffractometer.

(19) (a) Heywood, B. R.; Rajam, S.; Mann, S. *J. Chem. Soc., Faraday Trans.* **1991**, *87*, 735−743. (b) Sedlak, M.; Cölfen, H. *Macromol. Chem. Phys.* **2001**, *202*, 587−597.

(20) (a) Gehrke, N.; Cölfen, H.; Pinna, N.; Antonietti, M.; Nassif, N. *Cryst. Growth Des.* **2004**, *5*, 1317−1319. (b) Kojima, Y.; Sadomoto, A.; Yasue, T.; Arai, Y. *J. Ceram. Soc. Jpn.* **1992**, *100*, 1128−1135.

(21) Bujan, M.; Sikiriæ, M.; Filipoviæ-Vincekoviæ, N.; Vdoviæ, N.; Garti, N.; Füredi-Milhofer, H. *Langmuir* **2001**, *17*, 6461−6470.

(22) Nassif, N.; Gehrke, N.; Pinna, N.; Shirshova, N.; Tauer, K.; Antonietti, M.; Cölfen H. *Angew. Chem., Int. Ed.* **2005**, *44*, 6004−6009.

(23) (a) Sugimoto, T. *Adv. Colloid Interface Sci.* **1987**, *28*, 65−108. (b) Penn, R. L. *J. Phys. Chem. B* **2004**, *108*, 12707−12712.

(24) (a) Tang, Z. Y.; Kotov, N. A.; Giersig, M. *Science* **2002**, *297*, 237−240. (b) Liu, B.; Yu, S.-H.; Li, L.; Zhang, F.; Zhang, Q.; Yoshimura, M.; Shen, P. *J. Phys. Chem. B* **2004**, *108*, 2788−2792.

(25) (a) Faatz, M.; Gröhn, F.; Wegner, G. *Adv. Mater.* **2004**, *16*, 996−1000. (b) Xu, X.; Han, J. T.; Cho, K. *Langmuir* **2005**, *21*, 4801−4804.